Journal of Polymers and the Environment (2020) 28:1095–1105
https://doi.org/10.1007/s10924-020-01671-5

ORIGINAL PAPER

Mesoporous Crosslinked Chitosan-Activated Charcoal Composite for the Removal of Thionine Cationic Dye: Comprehensive Adsorption and Mechanism Study

Ali H. Jawad[1] · **Ahmed Saud Abdulhameed**[3] · **Mohd Sufri Mastuli**[1,2]

Published online: 5 February 2020

Abstract
Chitosan (CS) was coalesced with activated charcoal (AC), followed by crosslinking reaction with epichlorohydrin (ECH) to form a mesoporous crosslinked chitosan–epichlorohydrin/activated charcoal composite (CS-ECH/AC). The structural and physicochemical properties of CS-ECH/AC were characterized by Brunauer–Emmett–Teller, X-ray diffraction, scanning electron microscopy, Fourier transform infrared spectroscopy, and point-of-zero charge (pH_{PZC}) analyses. CS-ECH/AC was used to remove thionine (TH), a model cationic dye, from aqueous solution. Batch mode adsorption studies were performed by varying operational adsorption parameters, such as adsorbent dosage (0.04–0.30 g), solution pH (3–11), initial TH dye concentrations (10–100 mg/L), and contact time (0–270 min). The equilibrium data was described well by the Freundlich isotherm, and the maximum adsorption capacity of CS-ECH/AC for TH dye adsorption was 60.9 mg/g at 303 K. The kinetic uptake profiles were well described by the pseudo-second-order model. Thermodynamics results indicated a spontaneous and exothermic adsorption process. The proposed adsorption mechanism included mostly electrostatic attractions, H-bonding interactions, and π–π interactions. All these results showed that CS-ECH/AC can be considered as a feasible biocomposite material for the removal of cationic dyes from wastewater.

Keywords Chitosan · Activated charcoal · Epichlorohydrin · Thionine dye · Adsorption mechanism

Introduction

The use of organic dyes as coloring agents has become extensive, particularly in the textile, printing, leather, paint, food, and cosmetics industries [1]. The discharge of these dyes into water bodies without treatment is one of the most important environmental problems because of its risks on environmental safety and human health [2]. Therefore, these dyes should be removed before being discharged into the environment. Various techniques have been applied to treat dye-containing water and wastewater, such as adsorption [3, 4], electrochemical oxidation [5], biological treatment [6], and coagulation [7]. Among these treatment techniques, adsorption is one of the most efficient methods that is used for the removal of pollutants due to its advantages such as high efficiency, low cost, simplicity of design, and nongeneration of toxic materials [8–11].

Chitosan (CS) is the most-used biological molecule in the adsorption of several water pollutants because of its many preferable properties such as biodegradability, biocompatibility, and adsorption ability [12, 13]. The adsorption ability of CS can be attributed to the presence of reactive functional groups of amino ($–NH_2$) and hydroxyl (–OH) in its molecular structure [14]. These groups are considered active adsorption sites in wastewater treatment technologies to remove different pollutants, such as dyes and metals, through various mechanisms, including electrostatic attractions, H interactions, and chemical interactions [15–19]. However, the application of CS as an adsorbent in wastewater treatment technologies is still limited by its high solubility in acidic environment, leachability, poor mechanical properties,

✉ Ali H. Jawad
ali288@uitm.edu.my; ahjm72@gmail.com

[1] Faculty of Applied Sciences, Universiti Teknologi MARA, 40450 Shah Alam, Selangor, Malaysia

[2] Centre for Nanomaterials Research, Institute of Science, Uviversiti Teknologi MARA, 40450 Shah Alam, Selangor, Malaysia

[3] Chemistry Department, College of Science, University of Anbar, Ramadi, Iraq

and swelling in aqueous medium [20]. A highly effective pathway to overcoming these limitations and enhancing the physiochemical properties of the CS biopolymer is chemical modification by crosslinking reaction and/or composting with activated charcoal (AC) [21–24].

Generally, crosslinking reaction is a convenient method to improve the chemical stability of CS in acidic media and reduce its hydrophobicity [25]. Composting CS with AC is another distinguished method that can be applied to improve the surface property, porosity, and adsorptive property of the CS biopolymer [23]. AC is a porous material composed of C that is arranged in a quasi-graphitic form [26]. AC exhibits many preferable properties when it is used as an adsorbent, such as large surface area and fine network of pores [27]. At present, composite CS-AC derivatives exhibit multifunctional performances for unlimited promising applications, such as dye removal [28], metal ion removal [29], antibiotics [30], H storage [31], CO_2 capture [32], antibacterial activity [33], and catalyst [34].

Thus, the objective of this study is to develop hybrid crosslinked CS epichlorohydrin/AC composite (CS-ECH/AC) by coalescing CS-ECH with AC to form a promising composite biosorbent as a suitable candidate for the removal of cationic dyes, such as thionine (TH) dye, from an aqueous environment. The adsorption key parameters, such as adsorbent dosage, solution pH, TH dye concentration, and contact time on adsorption of TH were optimized. The adsorption isotherm and kinetics were also determined. Thermodynamic functions, such as Gibb's free energy (ΔG°), enthalpy (ΔH°), and entropy (ΔS°) were also investigated. The adsorption mechanism of TH dye on the CS-ECH/AC surface was also discussed.

Materials and Methods

Materials

CS with a medium molecular weight, deacetylation degree of 68%, and ≥ 98% (w/v) aqueous solution epichlorohydrin (ECH) were obtained from Sigma–Aldrich. AC powder was purchased from Fluka. TH dye ($C_{12}H_{10}ClN_3S$, MW: 263.75 g/mol, λmax = 569 nm), HCl, NaOH, and acetic acid were purchased from R&M Chemicals. All the experiments in this research were performed using ultrapure water.

CS-ECH/AC Preparation

A total of 1.5 g CS flakes and 0.5 g AC powder were added in acetic acid (50 mL, 5% v/v). The solution was left for 24 h at room temperature with gentle stirring to ensure CS dissolution and mix AC powder. The resultant solution was injected into a beaker containing 1000 mL of NaOH (0.5 M) by syringe needle (10 mL) as drops, where the CS-AC beads formed instantaneously. The fresh beads of CS-AC were washed with distilled water for the removal of the trace amounts of NaOH solution. The crosslinking step was carried out by adding 90 mL of 1% ECH to the CS-AC beads on a thermostat water bath shaker at 40 °C for 2 h. Then, the CS-ECH/AC beads were washed with distilled water and air dried overnight. Afterwards, the CS-ECH/AC beads were converted to powder form by mortar and dried constantly in an oven. Finally, the CS-ECH/AC powder was sieved to the constant particle size of ≤ 250 µm before being used in the adsorption experiments. The proposed CS-ECH/AC is presented in Fig. 1.

CS-ECH/AC Characterization

The CS-ECH/AC was characterized by various analytical methods and techniques. The surface area and pore structure of the CS-ECH/AC were calculated by N_2 adsorption/desorption isotherms at 77 K using the Micromeritics ASAP 2020 analyzer. The crystalline nature of CS-ECH/AC was analyzed by X-Ray diffraction (XRD; model X'Pert PRO, PAnalytical). Scanning electron microscope (SEM; Zeiss Supra 40 VP, Germany) was used to investigate the surface morphology of CS-ECH/AC before and after TH adsorption. The pH of CS-ECH/AC at the point of zero charge (pHpzc) was calculated according to the published method [35]. Fourier Transform Infrared (FTIR) spectrometer (Perkin-Elmer, Spectrum RX I) was used to identify the functional groups of CS-ECH/AC before and after TH adsorption.

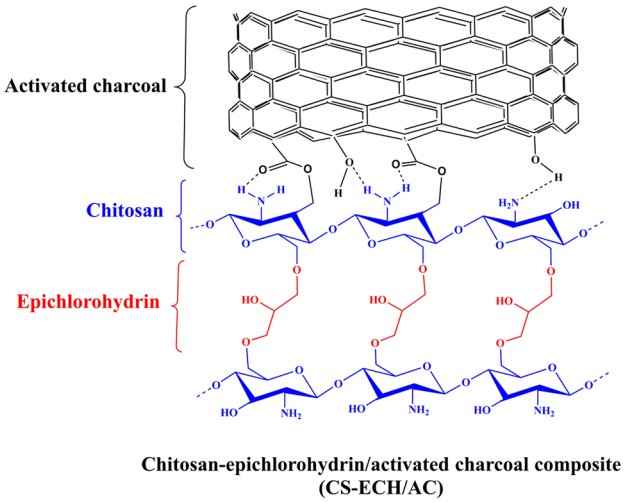

Fig. 1 The proposed molecular structure of CS-ECH/AC composite

Batch Adsorption Experiments

The adsorption of the TH dye on CS-ECH/AC was investigated in a batch mode. The experiments were carried out in a series of Erlenmeyer flasks (250 mL) containing 100 mL of TH dye solution with different initial TH dye concentrations (10–100 mg/L). The different dosages of CS-ECH/AC (0.04 to 0.3 g) were added to 100 mL of TH dye solution with different levels of solution pH (3–11), and agitated at fixed shaking speed of 110 strokes/min at 303 K using an isothermal water bath shaker (model WNB7-45, Memmert, Germany). Afterwards, syringe filtering (0.20 µm) was used to separate the adsorbents, and the initial and final TH dye concentrations were measured by using a UV–vis spectrophotometer (HACH DR 2800) at the maximum wavelength of 569 nm. Equilibrium isotherms were performed at optimum conditions (temperature = 303 K, adsorbent dosage = 0.18 g/100 mL, and solution pH 10) using initial TH concentrations ranging from 10 mg/L to 100 mg/L. The TH dye removal (*DR%*) and adsorbed amount of TH dye at equilibrium, that is, q_e (mg/g), were determined using Eqs. 1 and 2, respectively, as follows:

$$DR\% = \frac{(C_o - C_e)}{C_o} \times 100, \tag{1}$$

$$q_e = \frac{(C_o - C_e)V}{W}, \tag{2}$$

where C_o (mg/L) is the initial TH dye concentration, C_e (mg/L) is the TH dye concentration at equilibrium, V is the volume of the dye solution (L), and W is the amount of CS-ECH/AC (g).

Results and Discussion

Characterization

Physicochemical Properties of CS-ECH/AC

The pore structure and specific surface area of CS-ECH/AC were determined by N_2 adsorption/desorption isotherms, as depicted in Fig. 2. As shown in the figure, the N_2 physisorption isotherm was type IV according to the IUPAC classification. This result indicated the presence of mesopores in the CS-ECH/AC structure. The textural properties of the synthesized CS-ECH/AC are presented in Table 1. According to Table 1, the mean pore diameter of CS-ECH/AC was 3.69 nm, thereby indicating that the CS-ECH/AC is a mesoporous material [36]. The results also showed that the surface area of CS-ECH/AS was 49.3 m^2/g. This relatively high surface area of CS-ECH/AS can be attributed to the loading of AC into the polymeric matrix of CS-ECH, and the mesoporous structure of CS-ECH/AC would be responsible for the enhancement of the adsorption of TH molecules on the CS-ECH/AC surface because of the high diffusion of TH molecules through the mesoporous structure of the adsorbent [37].

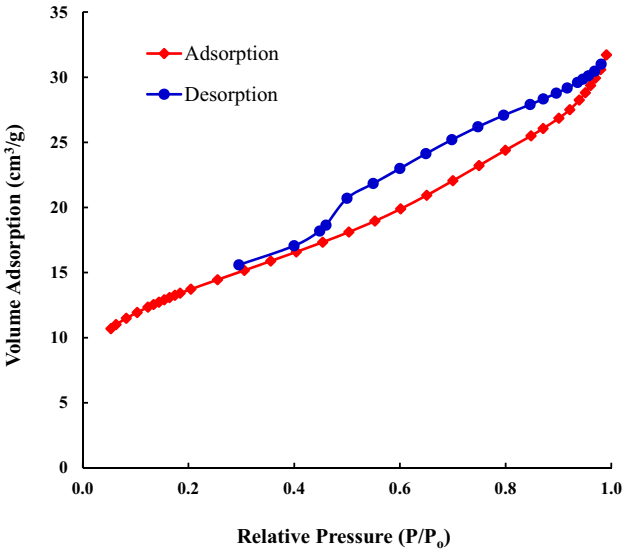

Fig. 2 N_2 adsorption–desorption isotherms of CS-ECH/AC

Table 1 The textural properties of CS-ECH/AC

Surface property	Value
BET surface area (m^2/g)	49.3
Total pore volume (cm^3/g)	0.048
Mean pore diameter (nm)	3.96
Monolayer capacity (cm^3/g)	11.3

XRD Analysis

XRD analysis was carried out to determine the crystalline and/or amorphous nature of CS-ECH/AC, as shown in Fig. 3a. As shown in the figure, the sharp and broad diffraction peaks at $2\theta = 24°$ (002) and $2\theta = 42°$ (100) were recorded. This result can be attributed to the typical crystalline regions of CS-ECH/AC, which are established through intramolecular and intermolecular H-bonding interactions [38, 39].

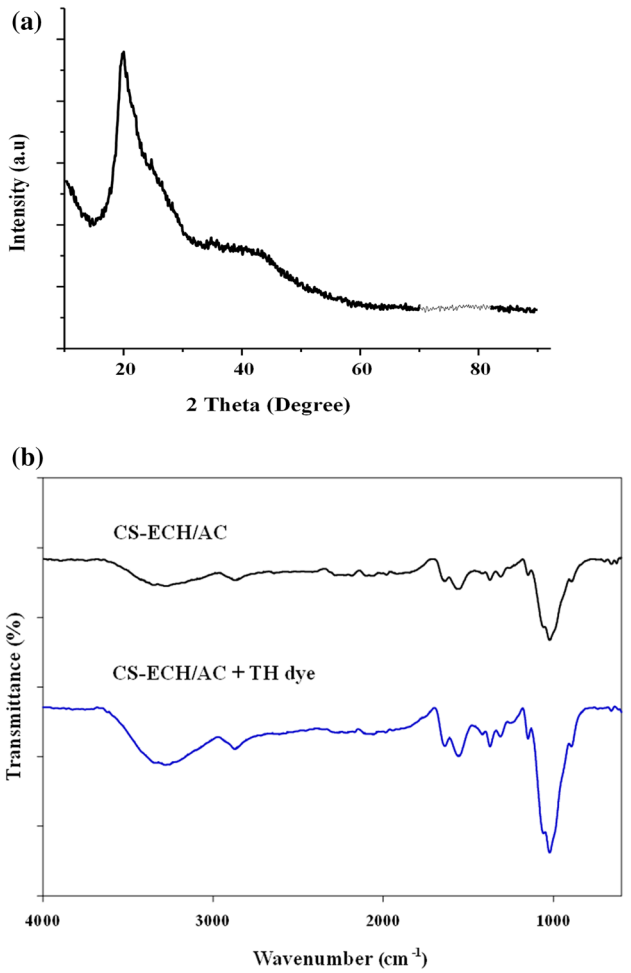

Fig. 3 **a** XRD pattern of CS-ECH/AC, and **b** FTIR spectra of CS-ECH/AC, and CS-ECH/AC after TH adsorption

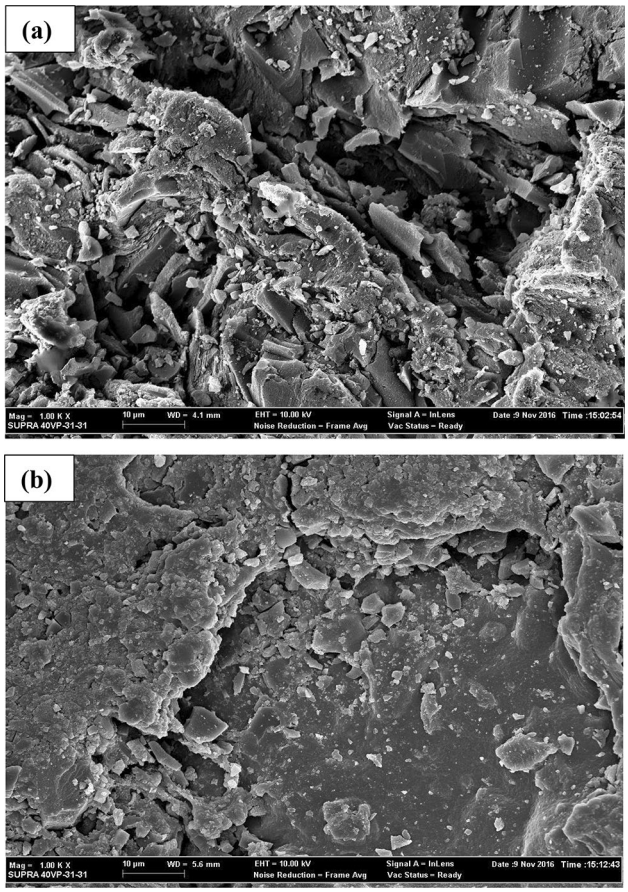

Fig. 4 SEM images of **a** CS-ECH/AC, and **b** CS-ECH/AC after TH dye adsorption

FTIR Spectral Analysis

FTIR analysis was performed to determine the functional groups on CS-ECH/AC surface before and after TH adsorption. Figure 3b shows the FTIR spectra of CS-ECH/AC and CS-ECH/AC after TH dye adsorption. The CS-ECH/AC spectrum showed that distinguished characteristic peaks can be assigned as follows: 3400 (stretching vibrations of –NH and –OH bonds), 2870 (stretching vibrations of C–H in –CH and $–CH_2$), 1700 (vibrations of C=O bond in RCOOH or RCOOR), 1650 (bending vibration of N–H), 1500 (vibrations of C=C bond in aromatic rings), 1380 (stretching vibration of C–N), and 1090 cm^{-1} (skeletal vibration of C–O) [30, 32]. These peaks showed that the AC was successfully grafted with the chains of CS-ECH and confirmed the chemical interactions, including esterification and H bonding between functional groups of the CS and O groups of AC [29], as shown in Fig. 3. The FTIR spectrum of CS-ECH/AC after TH adsorption showed evident shift in several peaks to high wavenumbers, thereby indicating the interactions between functional groups of the CS-ECH/AC and TH dye molecules that are loaded on the CS-ECH/AC surface.

SEM Analysis

SEM analysis was performed to investigate the surface morphology of CS-ECH/AC before and after the adsorption of the TH molecules. Figure 4a and 4b shows the SEM images of CS-ECH/AC and CS-ECH/AC after TH adsorption, respectively. Figure 4a shows that the surface morphology of CS-ECH/AC was a rough and heterogonous surface with evident cavities and irregular pore size. The presence of these pores within the CS-ECH/AC structure can play an essential role in the adsorption process of the TH molecules. The CS-ECH/AC surface after TH dye absorption (Fig. 4b) was less porous and compact with the disappearance of cavities on the CS-ECH/AC surface, thereby indicating that the TH molecules were successfully loaded on the CS-ECH/AC surface.

Adsorption Study

Effect of CS-ECH/AC Dosage

The effect of CS-ECH/AC dosage on TH dye removal by CS-ECH/AC was investigated by varying the adsorbent dosage from 0.04 to 0.3 g and fixing the volume, initial TH concentration, temperature, contact time, and shaking speed at 100 mL, 50 mg/L, 303 K, 600 min, and 110 strokes/min, respectively, as shown in Fig. 5a. The percentage of TH removal increased from 37.7% to 92.9% with increased CS-ECH/AC dosage from 0.04 to 0.18 g/100 mL (0.02 g to 0.2 g). This increase in TH removal with increased CS-ECH/AC dosage may be due the increase in available surface area of CS-ECH/AC in TH solution. A high adsorbent dosage also had a large number of active adsorption sites available for TH molecule adsorption. Further increase in CS-ECH/AC dosage did not result in any remarkable change in the TH dye removal. Therefore, 0.18 g/100 mL was selected as the optimum CS-ECH/AC dosage for further experiments.

Effect of Solution pH

The effect of initial pH on the adsorption capacity (q_t) of TH onto CS-ECH/AC was examined at different levels (pH 3–11) by fixing other parameters (adsorbent dosage of 0.18 g/100 mL, TH dye concentration of 50 mg/L, and temperature of 303 K), as shown in Fig. 5b. However, as illustrated in Fig. 5b, TH uptake (q_e) onto CS-ECH/AC was not considerably affected by pH within the range of 6–11 because of the buffering effect of the adsorbent, and a slight decrease in q_t can be observed in an acidic environment. The recorded pHpzc of CS-ECH/AC was 7, as shown in Fig. 5c. The CS-ECH/AC surface would be negatively charged at a basic pH environment of 7 or above. Thus, a strong electrostatic attraction can occur between the positively charged groups of TH and negatively charged groups on the CS-ECH/AC surface. Therefore, pH 7 was selected as the optimum pH for further experiments.

Effect of Temperature

The temperature is a fundamental adsorption parameter that plays an important role in the adsorption process. The effect of temperature (303, 313, and 323 K) on the q_t of TH dye by CS-ECH/AC was investigated at initial RR120 concentration (50 mg/L), solution pH (10), and adsorbent dosage (0.18 g/100 mL), as shown in Fig. 5d. The results showed that the changes in temperature were not significant on the adsorption of TH dye by CS-ECH/

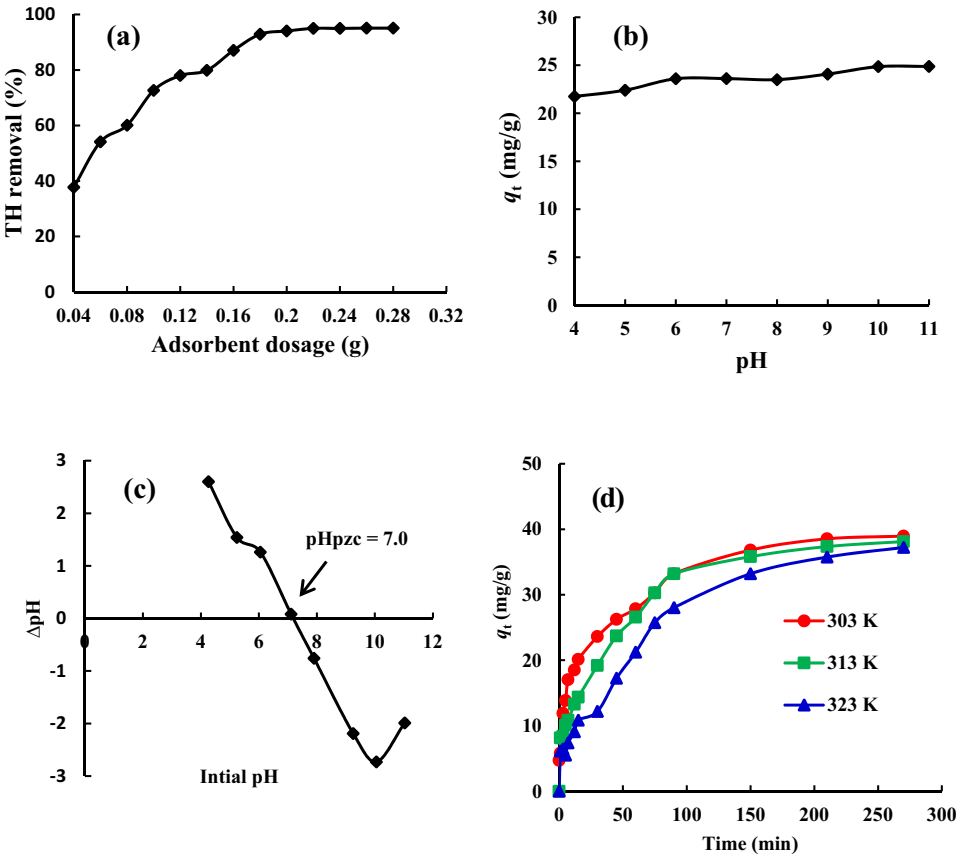

Fig. 5 **a**Effect of adsorbent dosage on removal of TH dye, **b** effect of pH on the adsorption of TH dye, **c** pHpzc of CS-ECH/AC, and **d** effect of temperature on the adsorption of TH dye

AC. However, a slight decrease in the q_t was observed by increasing the temperature up to 323 K that can be attributed to the exothermic nature of the adsorption process [40].

Effects of Initial TH Concentration and Contact Time

The effects of initial TH concentration and contact time on adsorption equilibrium were investigated. The q_t(mg/g) against time at different initial TH dye concentrations of 10, 20, 40, 60, 80 and 100 mg/L is shown in Fig. 6. Other optimum key parameters, such as adsorbent dose = 0.18 g, solution pH 7, and temperature = 303 K, remained constant within this part of the study. Figure 6 shows that the quantity of the TH dye molecule uptake onto CS-ECH/AC surface increased from 5.74 to 45.6 mg/g with an increase in the initial TH dye concentrations from 10 to 100 mg/L. This result can be attributed to the high concentration gradient, which provided a driving force to move the TH dye molecules toward active adsorption sites [41].

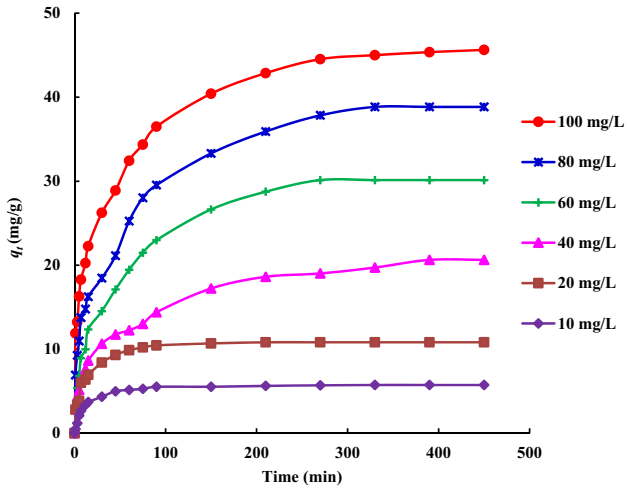

Fig. 6 Influence of initial TH dye concentration and contact time on adsorption of TH dye by CS-ECH/AC (volume of solution = 100 mL, temperature = 303 K, pH = 7, adsorbent dosage = 0.18 g)

Kinetic Modeling

To identify the mechanism of the TH dye adsorption onto CS-ECH/AC, we applied the kinetic models of the pseudo-first-order (PFO) and -second-order (PSO) were applied to examine the experimental results of different initial TH dye concentrations. The nonlinear forms of the PFO [42] and PSO [43] models are expressed by Eqs. 3 and 4, respectively, as follows:

$$q_t = q_e\left(1 - \exp^{-k_1 t}\right) \tag{3}$$

$$qt = \frac{q_e^2 k_2 t}{1 + q_e k_2 t} \tag{4}$$

where q_e (mg/g) is the amount of TH adsorbed by CS-ECH/AC at equilibrium; q_t (mg/g) is the amount of TH adsorbed by CS-ECH/AC at time (t); and k_1 (1/min) and k_2 (g/mg min) are the rate constants of PFO and PSO, respectively. The kinetic parameters of the PFO and PSO models are presented in Table 2. The results (Table 2) showed that the adsorption process of the TH by the CS-ECH/AC fits PSO model because of the high correlation coefficient (R^2) values. The calculated q_e values from PSO model was close to experimental results of q_e, thereby suggesting that the adsorption of TH dye on the CS-ECH/AC surface involved chemical interactions, such as electrostatic attraction between the positive charge of TH dye and negative charge available on the CS-ECH/AC surface [44].

Isotherm Modelling

Adsorption isotherms are important tools to describe the interactions between the adsorbate and CS-ECH/AC adsorbent [45, 46]. The three isotherm models of Langmuir, Freundlich, and Temkin were applied to investigate the equilibrium isotherms of adsorption and calculating the q_{max}. The Langmuir model [47] is presented by Eq. 5:

Table 2 PFO and PSO kinetic parameters for TH dye adsorption on CS-ECH/AC

C_o (mg/L)	$q_{e\,exp}$ (mg/g)	PFO			PSO		
		$q_{e\,cal}$ (mg/g)	k_1 (1/min)	R^2	$q_{e\,cal}$ (mg/g)	$k_2 \times 10^{-2}$ (g/mg min)	R^2
10	5.7	5.4	0.078	0.98	5.9	1.8	0.99
20	10.8	10.3	0.09	0.94	11	1.2	0.98
40	20.6	18.7	0.025	0.89	20.4	0.19	0.95
60	30.1	28.9	0.023	0.94	31.9	0.1	0.97
80	38.8	36.3	0.026	0.88	39.4	0.1	0.94
100	45.5	40.6	0.05	0.84	44.2	0.16	0.92

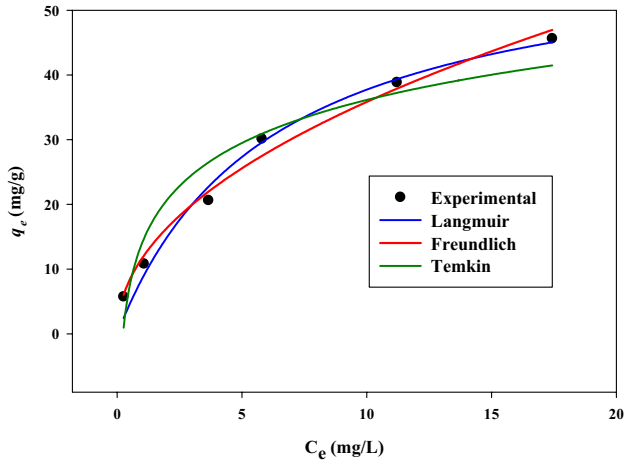

Fig. 7 Isotherm models plots of Langmuir, Freundlich, and Temkin, for the adsorption of TH dye on CS-ECH/AC at 303 K (pH = 7, adsorbent dosage = 0.18 g, and volume of solution = 100 mL)

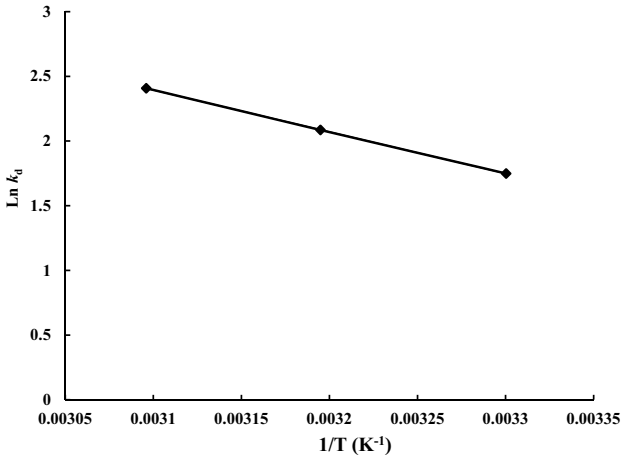

Fig. 8 Van't Hoff plot for TH dye adsorption onto CS-ECH/AC (pH = 7, adsorbent dose = 0.18 g, and volume of solution = 100 mL)

Table 3 Parameters of the isotherm models for TH dye adsorption on CS-ECH/AC at 303 K

Adsorption isotherm	Parameter	Value
Langmuir	q_m (mg/g)	60.9
	K_a (L/mg)	0.16
	R^2	0.98
Freundlich	K_f (mg/g) $(L/mg)^{1/n}$	11.7
	n	2.05
	R^2	0.99
Temkin	K_T (L/mg)	1.46
	b_T (J/mol)	262.6
	R^2	0.92

$$q_e = \frac{q_{\max} K_a C_e}{1 + K_a C_e} \tag{5}$$

where q_e (mg/g), $q_{\max}$ (mg/g), C_e (mg/L), and K_a (L/mg) are uptake amount of dye at equilibrium, dye concentration at equilibrium, Langmuir maximum adsorption capacity, and Langmuir constant, respectively. The Freundlich model [48] is provided by Eq. 6, as follows:

$$q_e = K_f C_e^{1/n} \tag{6}$$

where K_f ([mg/g] $[L/mg]^{1/n}$) and n are Freundlich constant and adsorption intensity, respectively. The Temkin isotherm model [49] is expressed by Eq. 7:

$$q_e = \frac{RT}{b_T} \ln\left(K_T C_e\right) \tag{7}$$

where K_T (L/mg), R (8.314 J/mol K), T (K), and b_T (J/mol) are Temkin constant, universal gas constant, absolute temperature, and heat of adsorption, respectively.

The nonlinear plots of the studied isotherm models resulting from Eqs. 5–7 are displayed in Fig. 7. The isotherm parameters of the models are presented in Table 3. According to the R^2 values (Table 3) obtained from the isotherm models, the Freundlich isotherm had highest R^2 of 0.99, which suggested the multilayer adsorption of TH dye

Table 4 Comparison of the adsorption capacity of cationic dyes by various adsorbents

Adsorbent	Dye	q_m (mg/g)	References
Cotton fiber based Schiff base	Rhodamine 6G	696.4	[51]
Magnetic Fe_3O_4/nitrogen doped-porous carbon nanocomposite	Thionine	450.78	[52]
Acid-treated rubber leaf	Methylene blue	263.2	[53]
Mesoporous Iraqi red kaolin clay	Methylene blue	240.4	[54]
Modified coal fly ash with sulfonic acid	Malachite green	233.3	[55]
Commercial coconut shell activated carbon	Methylene blue	149.25	[56]
Mesoporous-activated carbon	Methylene blue	143.53	[57]
Magnetite nanoparticles loaded tea waste	Thionine	128.21	[58]
Magnetic multi-wall carbon nanotubes	Thionine	36.63	[59]
H_2SO_4 magnetic chitosan nanocomposite	Methylene blue	20.41	[60]
Crosslinked chitosan/activated charcoal composite	Thionine	60.9	This study

Table 5 Thermodynamic parameters for the adsorption of TH dye on CS-ECH/AC

T (K)	k_d	ΔG° (kJ/mol)	ΔH° (kJ/mol)	ΔS° (kJ/molK)
303	11.1	−41.4	−31.0	0.116
313	8.0	−40.2		
323	5.7	−39.0		

adsorption onto the CS-ECH/AC [50]. The q_{max} of CS-ECH/AC for TH was 60.9 mg/g. The q_t of CS-ECH/AC for TH dye was compared with other adsorbents used for the removal of various cationic dyes, as presented in Table 4. As shown in the table, the reasonable q_t of CS-ECH/AC indicated a potential application of CS-ECH/AC adsorbent as a promising renewable adsorbent for cationic dye removal from an aqueous environment .

Adsorption Thermodynamics

Thermodynamic study was performed to investigate the spontaneity and feasibility of the adsorption process and freedom degree of the adsorbed TH dye at the solid/solution interface. The adsorption thermodynamic functions of the adsorbed TH dye by CS- ECH/AC, such as ΔG°, ΔH°, and ΔS°, were calculated by Eqs. 8–10 [61]:

$$\Delta G^{\circ} = -RTlnK_d, \tag{8}$$

$$k_d = \frac{q_e}{C_e}, \tag{9}$$

$$lnk_d = \frac{\Delta S^{\circ}}{R} - \frac{\Delta H^{\circ}}{RT} \tag{10}$$

The ΔH° and ΔS° values were calculated from the slope and intercept of the Van't Hoff plot of *ln kd* versus *1/T*, as shown Fig. 8. The thermodynamic functions are presented in Table 5. The results showed a negative value of the ΔG° and a negative value of the ΔH°, thereby indicating that the adsorption process was spontaneous and exothermic in nature, respectively [34]. The randomness at the

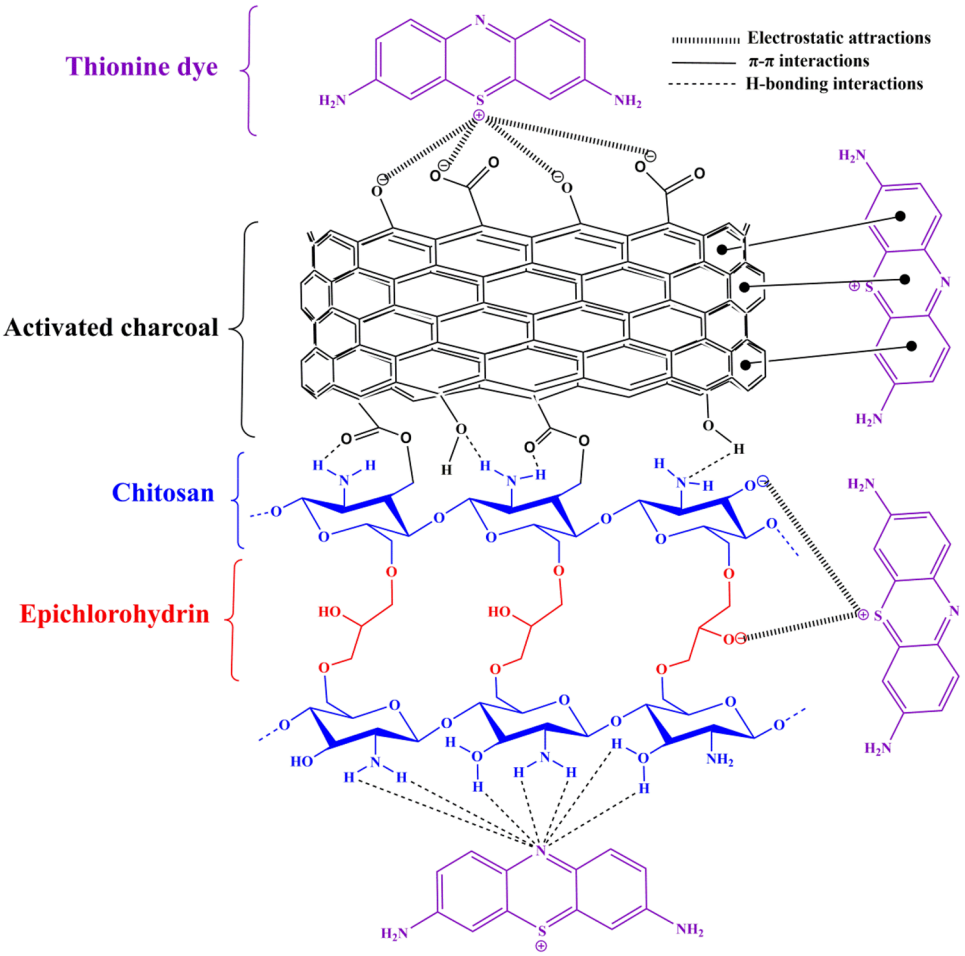

Fig. 9 Illustration of the possible interaction between CS-ECH/AC and TH dye including electrostatic attraction, H-bonding interaction, and π–π interactions

solid–solution interface is expected to increase because of the positive ΔS°.

Adsorption Mechanism

The adsorption mechanism of TH onto CS-ECH/AC surface can be attributed to different types of interactions, as shown in Fig. 9. The mechanism involved the electrostatic interaction between positively charged groups of the TH dye with negatively charged groups available on the CS-ECH/AC surface. Adsorption mechanism also included H-bonding interactions between H in the CS-ECH/AC surface and N atoms in the TH dye structure. Finally, π–π interaction can occur between the hexagonal skeleton of AC and aromatic rings of TH. According to the possibilities mentioned above, these interactions were responsible for enhancing the adsorption process of TH on the CS-ECH/AC surface. Similar observations were reported by other researchers for the adsorption of cationic dyes by magnetic CS/AC composite [62] and CS crosslinked graphene oxide/lignosulfonate composite [1].

Conclusion

Mesoporous crosslinked CS-ECH/AC composite was successfully synthesized and applied as an effective adsorbent to remove TH dye (cationic dye) from aqueous solution. The optimum adsorption conditions were the adsorbent dosage of 0.18 g/100 mL, solution pH of 7, and temperature of 303 K. The maximum q_t of CS-ECH/AC obtained from Langmuir model was 60.9 mg/g. Thermodynamics results indicated that the adsorption process was spontaneous and exothermic in nature. The adsorption mechanism of the TH dye on CS-ECH/AC surface can be assigned to various types of interactions, such as electrostatic attraction, H-bonding interaction, and π–π interaction. The adsorption results indicated that CS-ECH/AC can be considered as a feasible and promising biocomposite adsorbent for the removal of cationic dyes from an aqueous environment.

Acknowledgements The authors would like to thank the Universiti Teknologi MARA, Institute of Research Management and Innovation (Institut Pengurusan Penyelidikan & Inovasi) for supporting this project under LESTARI grant (600-IRMI 5/3/LESTARI (037/2019)).

References

1. Yan M, Huang W, Li Z (2019) Chitosan cross-linked graphene oxide/lignosulfonate composite aerogel for enhanced adsorption of methylene blue in water. Int J Biol Macromol 136:927–935
2. Meili L, Lins PVS, Costa MT, Almeida RL, Abud AKS, Soletti JI, Erto A (2019) Adsorption of methylene blue on agroindustrial wastes: experimental investigation and phenomenological modelling. Prog Biophys Mol Biol 141:60–71
3. Karimifard S, Alavi Moghaddam MR (2016) Removal of an anionic reactive dye from aqueous solution using functionalized multi-walled carbon nanotubes: isotherm and kinetic studies. Desalin. Water Treat. 57(35):16643–16652
4. Karimifard S, Alavi Moghaddam MR (2016) The effects of microwave regeneration on adsorptive performance of functionalized carbon nanotubes. Water Sci. Technol. 73(11):2638–2643
5. Wang J, Yao J, Wang L, Xue Q, Pan B (2019) Multivariate optimization of the pulse electrochemical oxidation for treating recalcitrant dye wastewater. Sep. Purif. Technol. 230:115851
6. Liu J, Liu A, Wang W, Li R, Zhang WX (2019) Feasibility of nanoscale zero-valent iron (nZVI) for enhanced biological treatment of organic dyes. Chemosphere 237:124470
7. Huang Z, Wang T, Shen M, Huang Z, Chong Y, Cui L (2019) Coagulation treatment of swine wastewater by the method of in-situ forming layered double hydroxides and sludge recycling for preparation of biochar composite catalyst. Chem Eng J 369:784–792
8. Abdulhameed AS, Mohammad AT, Jawad AH (2019) Application of response surface methodology for enhanced synthesis of chitosan tripolyphosphate/TiO_2 nanocomposite and adsorption of reactive orange 16 dye. J Clean Prod 232:43–56
9. Li Z, Sellaoui L, Dotto GL, Bonilla-Petriciolet A, Lamine AB (2019) Understanding the adsorption mechanism of phenol and 2-nitrophenol on a biopolymer-based biochar in single and binary systems via advanced modeling analysis. Chem Eng J 371:1–6
10. Li Z, Dotto GL, Bajahzar A, Sellaoui L, Belmabrouk H, Lamine AB, Bonilla-Petriciolet A (2019) Adsorption of indium (III) from aqueous solution on raw, ultrasound-and supercritical-modified chitin: Experimental and theoretical analysis. Chem Eng J 373:1247–1253
11. Li Z, Gómez-Avilés A, Sellaoui L, Bedia J, Bonilla-Petriciolet A, Belver C (2019) Adsorption of ibuprofen on organo-sepiolite and on zeolite/sepiolite heterostructure: Synthesis, characterization and statistical physics modeling. Chem Eng J 371:868–875
12. Jawad AH, Norrahma SSA, Hameed BH, Ismail K (2019) Chitosan-glyoxal film as a superior adsorbent for two structurally different reactive and acid dyes: Adsorption and mechanism study. Int J Biol Macromol 135:569–581
13. Jawad AH, Nawi MA, Mohamed MH, Wilson LD (2017) Oxidation of chitosan in solution by photocatalysis and product characterization. J Polym Environ 25:828–835
14. Jawad AH, Mamat NH, Hameed BH, Ismail K (2019) Biofilm of cross-linked Chitosan-Ethylene Glycol Diglycidyl Ether for removal of Reactive Red 120 and Methyl Orange: Adsorption and mechanism studies. J Environ Chem Eng 7:102965
15. Hydari S, Sharififard H, Nabavinia M, Reza Parvizi M (2012) A comparative investigation on removal performances of commercial activated carbon, chitosan biosorbent and chitosan/activated carbon composite for cadmium. Chem. Eng. J. 193:276–282
16. Abdulhameed AS, Mohammad AT, Jawad AH (2019) Modeling and mechanism of reactive orange 16 dye adsorption by chitosan-glyoxal/ TiO_2 nanocomposite: application of response surface methodology. Desalin Water Treat 164:346–360
17. Abdulhameed AS, Jawad AH, Mohammad AT (2019) Synthesis of chitosan-ethylene glycol diglycidyl ether/TiO_2 nanoparticles for adsorption of reactive orange 16 dye using a response surface methodology approach. Bioresour Technol 293:122071
18. Zhang L, Sellaoui L, Franco D, Dotto GL, Bajahzar A, Belmabrouk H, Li Z (2020) Adsorption of dyes brilliant blue, sunset yellow and tartrazine from aqueous solution on chitosan: Analytical

interpretation via multilayer statistical physics model. Chem Eng J 382:122952
19. Li Z, Sellaoui L, Dotto GL, Lamine AB, Bonilla-Petriciolet A, Hanafy H, Erto A (2019) Interpretation of the adsorption mechanism of Reactive Black 5 and Ponceau 4R dyes on chitosan/polyamide nanofibers via advanced statistical physics model. J Mol Liq 285:165–170
20. Nawi MA, Jawad AH, Sabar S, Ngah WW (2011) Photocatalytic-oxidation of solid state chitosan by immobilized bilayer assembly of TiO_2–chitosan under a compact household fluorescent lamp irradiation. Carbohydr Polym 83(3):1146–1152
21. Jawad AH, Islam MA, Hameed BH (2017) Cross-linked chitosan thin film coated onto glass plate as an effective adsorbent for adsorption of reactive orange 16. Int J Biol Macromol 95:743–749
22. Mohammad AT, Abdulhameed AS, Jawad AH (2019) Box-Behnken design to optimize the synthesis of new crosslinked chitosan-glyoxal/TiO_2 nanocomposite: Methyl orange adsorption and mechanism studies. Int J Biol Macromol 129:98–109
23. Guo M, Wang J, Wang C, Strong PJ, Jiang P, Ok YS, Wang H (2019) Carbon nanotube-grafted chitosan and its adsorption capacity for phenol in aqueous solution. Sci Total Environ 682:340–347
24. Malek NNA, Jawad AH, Abdulhameed AS, Ismail K, Hameed BH (2020) New magnetic Schiff's base-chitosan-glyoxal/fly ash/Fe_3O_4 biocomposite for the removal of anionic azo dye: An optimized process. Int J Biol Macromol 146:530–539
25. Jawad AH, Mubarak NSA, Abdulhameed AS (2020) Tunable Schiff's base-cross-linked chitosan composite for the removal of reactive red 120 dye: Adsorption and mechanism study. Int J Biol Macromol 142:732–741
26. Thomas TD (2008) The role of activated charcoal in plant tissue culture. Biotechnol Adv 26(6):618–631
27. Roy S, Das P, Sengupta S, Manna S (2017) Calcium impregnated activated charcoal: Optimization and efficiency for the treatment of fluoride containing solution in batch and fixed bed reactor. Process Saf Environ 109:18–29
28. Pinho MT, Silva AM, Fathy NA, Attia AA, Gomes HT, Faria JL (2015) Activated carbon xerogel–chitosan composite materials for catalytic wet peroxide oxidation under intensified process conditions. J Environ Chem Eng 3(2):1243–1251
29. Sharififard H, Rezvanpanah E, Rad SH (2018) A novel natural chitosan/activated carbon/iron bio-nanocomposite: Sonochemical synthesis, characterization, and application for cadmium removal in batch and continuous adsorption process. Bioresour Technol 270:562–569
30. Danalıoğlu ST, Bayazit ŞS, Kuyumcu ÖK, Salam MA (2017) Efficient removal of antibiotics by a novel magnetic adsorbent: Magnetic activated carbon/chitosan (MACC) nanocomposite. J Mol Liq 240:589–596
31. Wróbel-Iwaniec I, Díez N, Gryglewicz G (2015) Chitosan-based highly activated carbons for hydrogen storage. Int J Hydrogen Energy 40(17):5788–5796
32. Jawad AH, Nawi MA (2012) Characterizations of the photocatalytically-oxidized cross-linked chitosan-glutaraldehyde and its application as a sub-layer in the TiO_2/CS-GLA bilayer photocatalyst system. J Polym Environ 20:817–829
33. Tang C, Hu D, Cao Q, Yan W, Xing B (2017) Silver nanoparticles-loaded activated carbon fibers using chitosan as binding agent: Preparation, mechanism, and their antibacterial activity. Appl Surf Sci 394:457–465
34. Wang L, Wang Y, Li A, Yang Y, Wang J, Zhao H, Qi T (2014) Electrocatalysis of carbon black-or chitosan-functionalized activated carbon nanotubes-supported Pd with a small amount of La_2O_3 towards methanol oxidation in alkaline media. Int J Hydrog Energy 39(27):14730–14738
35. Dalvand A, Nabizadeh R, Ganjali MR, Khoobi M, Nazmara S, Mahvi AH (2016) Modeling of Reactive Blue 19 azo dye removal from colored textile wastewater using L-arginine-functionalized Fe_3O_4 nanoparticles: Optimization, reusability, kinetic and equilibrium studies. J Magn Magn Mater 404:179–189
36. Sing KS (1985) Reporting physisorption data for gas/solid systems with special reference to the determination of surface area and porosity, (Recommendations 1984), Pure Appl. Chem. 57:603–619
37. Ahmed MJ, Okoye PU, Hummadi EH, Hameed BH (2019) High-performance porous biochar from the pyrolysis of natural and renewable seaweed (Gelidiella acerosa) and its application for the adsorption of methylene blue. Bioresour Technol 278:159–164
38. Qi X, Lin L, Shen L, Li Z, Qin T, Qian Y, Shen J (2019) Efficient decontamination of lead ions from wastewater by salecan polysaccharide-based hydrogels. ACS Sustain Chem Eng 7:11014–11023
39. Qi X, Liu R, Chen M, Li Z, Qin T, Qian Y, Shen J (2019) Removal of copper ions from water using polysaccharide-constructed hydrogels. Carbohydr Polym 209:101–110
40. Raghunath S, Anand K, Gengan RM, Nayunigari MK, Maity A (2016) Sorption isotherms, kinetic and optimization process of amino acid proline based polymer nanocomposite for the removal of selected textile dyes from industrial wastewater. J Photochem Photobiol B Biol 165:189–201
41. Njoku VO, Islam MA, Asif M, Hameed BH (2014) Preparation of mesoporous activated carbon from coconut frond for the adsorption of carbofuran insecticide. J Anal Appl Pyrol 110:172–180
42. Lagergren S (1898) Zur theorie der sogenannten adsorption geloster stoffe. Vet Akad Handl 24:1–39
43. Ho YS, McKay G (1998) Sorption of dye from aqueous solution by peat. Chem Eng J 70:115–124
44. Muthukumaran C, Sivakumar VM, Thirumarimurugan M (2016) Adsorption isotherms and kinetic studies of crystal violet dye removal from aqueous solution using surfactant modified magnetic nanoadsorbent. J Taiwan Inst Chem Eng 63:354–362
45. Qi X, Chen M, Qian Y, Liu M, Li Z, Shen L, Shen J (2019) Construction of macroporous salecan polysaccharide-based adsorbents for wastewater remediation. Int J Biol Macromol 132:429–438
46. Qi X, Wei W, Su T, Zhang J, Dong W (2018) Fabrication of a new polysaccharide-based adsorbent for water purification. Carbohydr Polym 195:368–377
47. Langmuir I (1918) The adsorption of gases on plane surfaces of glass, mica and platinum. J Am Chem Soc 40:1361–1403
48. Frenudlich HMF (1906) Over the adsorption in solution. J Phys Chem 57:385–471
49. Temkin MI (1940) Kinetics of ammonia synthesis on promoted iron catalysts. Acta Physiochim URSS 12:327–356
50. Qi X, Li Z, Shen L, Qin T, Qian Y, Zhao S, Shen J (2019) Highly efficient dye decontamination via microbial salecan polysaccharide-based gels. Carbohydr Polym 219:1–11
51. Agathian K, Kannammal L, Meenarathi B, Kailash S, Anbarasan R (2018) Synthesis, characterization and adsorption behavior of cotton fiber based Schiff base. Int J Biol Macromol 107:1102–1112
52. Nsabimana A, Kitte SA, Wu F, Qi L, Liu Z, Zafar MN, Xu G (2019) Multifunctional magnetic Fe_3O_4/nitrogen-doped porous carbon nanocomposites for removal of dyes and sensing applications. Appl Surf Sci 467:89–97
53. Jawad AH, Mallah SH, Mastuli MS (2018) Adsorption behavior of methylene blue on acid-treated rubber (Hevea brasiliensis) leaf. Desalin Water Treat 124:297–307
54. Jawad AH, Abdulhameed AS (2020) Mesoporous Iraqi red kaolin clay as an efficient adsorbent for methylene blue dye: Adsorption kinetic, isotherm and mechanism study. Surf Interface 18:100422
55. Dash S, Chaudhuri H, Gupta R, Nair UG (2018) Adsorption study of modified coal fly ash with sulfonic acid as a potential

adsorbent for the removal of toxic reactive dyes from aqueous solution: Kinetics and thermodynamics. J Environ Chem Eng 6(5):5897–5905
56. Rashid RA, Ishak MAM, Hello KM (2018) Adsorptive Removal of Methylene Blue by Commercial Coconut Shell Activated Carbon. Sci Lett 12:27–97
57. Marrakchi F, Ahmed MJ, Khanday WA, Asif M, Hameed BH (2017) Mesoporous-activated carbon prepared from chitosan flakes via single-step sodium hydroxide activation for the adsorption of methylene blue. Int J Biol Macromol 98:233–239
58. Madrakian T, Afkhami A, Ahmadi M (2012) Adsorption and kinetic studies of seven different organic dyes onto magnetite nanoparticles loaded tea waste and removal of them from wastewater samples. Spectrochim Acta A Mol Biomol Spectrosc 99:102–109
59. Madrakian T, Afkhami A, Ahmadi M, Bagheri H (2011) Removal of some cationic dyes from aqueous solutions using magnetic-modified multi-walled carbon nanotubes. J Hazard Mater 196:109–114
60. Rahmi, Ishmaturrahmi, Mustafa I (2019) Methylene blue removal from water using H_2SO_4 crosslinked magnetic chitosan nanocomposite beads. Microchem J 144:397–402
61. Jawad AH, Mubarak NSA, Abdulhameed AS (2019) Hybrid crosslinked chitosan epichlorohydrin/TiO_2 nanocomposite for reactive red 120 dye adsorption: kinetic, isotherm, thermodynamic, and mechanism study. J Polym Environ 28:624–637
62. Karaer H, Kaya I (2016) Synthesis, characterization of magnetic chitosan/active charcoal composite and using at the adsorption of methylene blue and reactive blue4. Micropor Mesopor Mater 232:26–38